

A balloon-borne cloud condensation nuclei counter

David J. Delene, Terry Deshler, Perry Wechsler, and Gabor A. Vali

Department of Atmospheric Science, University of Wyoming Laramie

Abstract. A balloon-borne instrument was constructed for observations of vertical profiles of cloud condensation nucleus (CCN) concentrations, active at 1% supersaturation. Droplet concentration in the static thermal-gradient diffusion chamber is deduced from the amount of scattered laser light detected by a photodetector. The photodetector is calibrated using a video camera and computer system to count the number of droplets produced from NaCl aerosol. Preliminary data are available from nine early morning profiles obtained at Laramie, Wyoming, between June 1995 and January 1997. To complement the CCN measurements, instruments that measure condensation nuclei (CN) and aerosols with diameter greater than $0.30\text{ }\mu\text{m}$ ($D_{0.3}$) were also included on the balloon package. CCN concentrations exhibited a general decrease from the surface to the top of the boundary layers, were generally uniform through well-mixed layers, and show variability above well-mixed layers. In general, the structure of the CCN profile appears to be closely related to the structure in the CN and $D_{0.3}$ profiles. Summer profiles generally have CCN concentration greater than 200 cm^{-3} up to 500 mbar, whereas winter profiles are less than 200 cm^{-3} at all levels.

1. Introduction

Despite over 40 years of research on cloud condensation nuclei (CCN), the sources and sinks of CCN are not well understood [Hudson, 1993]. The number concentration and activity of CCN influences cloud droplet spectra and hence precipitation processes and cloud albedo [Hobbs, 1993; Jennings, 1993]. It has been suggested that an increase in CCN concentration, due to increased SO_2 emissions, could offset temperature changes resulting from increased CO_2 concentrations [Wigley, 1989; Twomey, 1991].

Most studies of CCN have focused on measuring concentrations near the Earth's surface [Hudson and Squires, 1978; Hudson and Frisbie, 1991; Gras, 1995]; however, recent studies have used aircraft to obtain information on the spatial distribution of CCN [Hegg et al., 1995; Hudson and Svensson, 1995; Raga and Jonas, 1995]. Vertical distributions of CCN from aircraft measurements generally cover limited altitude ranges, so we have developed a balloon-borne CCN counter to extend these measurements. Recent balloon flights at Laramie, Wyoming, have provided vertical profiles of CCN concentrations at all levels of the troposphere. Some of these profiles along with the calibration procedure for the balloon-borne CCN counter are presented here.

2. CCN Counter Description

The balloon-borne CCN counter is similar to other static thermal-gradient diffusion chamber instruments [Lala and Justo, 1977; Bartlett and Ayers, 1981; Hoppel and Wojciechowski, 1981; Lala, 1981]. A 670 nm solid-state laser illuminates droplets as they grow within the chamber, and a photodetector measures the amount of scattered light.

The photodetector voltage is the primary measurement of the CCN counter and is recorded at 1 s intervals during balloon flights. A CCN measurement begins with a 5 s chamber flush to remove air from the previous sample. Next, an air sample is captured in the chamber, CCN are activated, droplets grow and fall out. The CCN concentration is determined during post processing based on calibration of the scattered light signal against known CCN concentration.

The diameter of the chamber is 75 mm, and the top and bottom plates are 12.5 mm apart. These dimensions allow for air in the chamber to reach equilibrium temperature distribution in about 3 s [Elliott, 1971]. Following the suggestion of Katz and Mirabel [1975], the temperature and vapor pressure between the top and the bottom plates are assumed to be linear. The top plate temperature is allowed to float with the enclosed temperature of the CCN counter, and the bottom plate is cooled. During balloon flights, the top plate temperature ranges from 10° to 30°C . The bottom plate temperature necessary to achieve the prescribed supersaturation is calculated before each sample based on a measurement of the top plate temperature. The temperature difference between the top and the bottom plates has to remain within 0.2°C of the prescribed value for 5 s before a measurement is initiated. Temperature fluctuation during measurements are usually $< 0.1^\circ\text{C}$, so the supersaturation, which was held at 1% for all data reported here, is constant within $\pm 0.05\%$ supersaturation. Both the top and the bottom plates are kept wet with saturated blotting papers. Laboratory tests and a balloon flight with ascent and descent temperatures at 40°C show that the blotter paper remains moist for the 2–3 hour duration of a balloon flight. Air samples are drawn into the chamber at 2.5 L/min. To avoid aerosol loss in stagnant air within the intake tube, air is drawn continuously though a bypass when the chamber is closed.

3. CCN Counter Calibration

Bench calibration of the CCN counter consists of establishing the relationship between the number of water

Copyright 1998 by the American Geophysical Union.

Paper number 98JD00053.
0148-0227/98/98JD-00053\$09.00

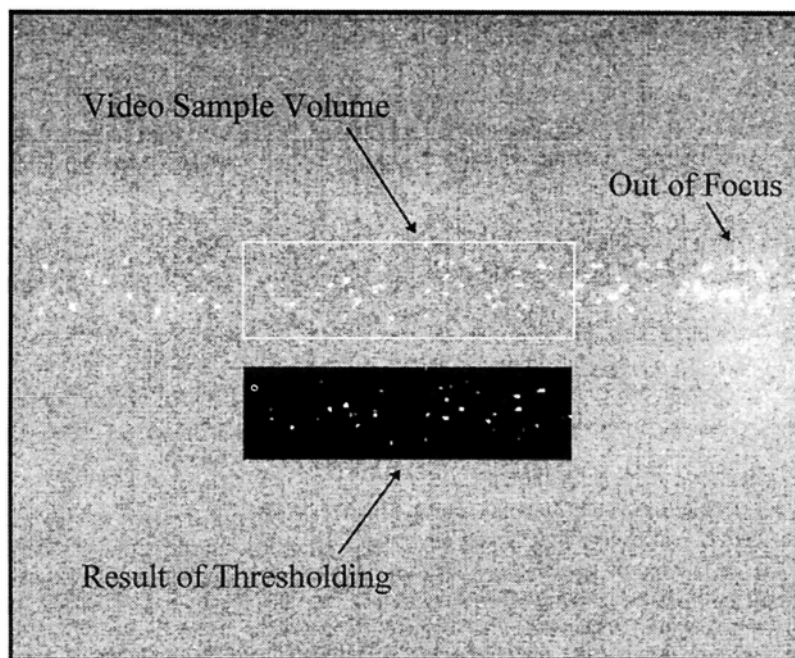


Figure 1. A typical video image of droplets in the static thermal-gradient diffusion chamber. The top part of the image is the raw gray scale digital image. The white rectangle outlines the area in which droplets are counted. Below, the gray scale image is the corresponding black and white image produced by applying the brightness threshold value.

droplets in the chamber and the photodetector voltage. To accomplish this requires counting the number of water droplets in a measured portion of the laser beam at the instant that the photodetector voltage is measured. Droplets growing within the chamber are imaged with a video camera and the resulting video data captured using a digital frame grabber. This enables the number of droplets within a defined video sample volume to be counted. The photodetector voltage is recorded concurrently with the video frame at 1 s intervals. The video sample volume is defined by a 10 mm segment of a 4 x 1 mm elliptical crosssection of the laser beam.

Divergence of the laser beam is negligible over the distance of the chamber, and the laser intensity falls off very rapidly at the edges, so fringe effects can be ignored. The longitudinal laser beam dimension was chosen as large as possible without including regions where droplets are out of focus. Although the video sample volume is not the same as the volume over which the photodetector collects scattered light, the two signals are proportional, as will be shown later.

To count droplets within the video sample volume, a brightness threshold value is set which defines pixels as either being bright enough to be part of a droplet or not part of a

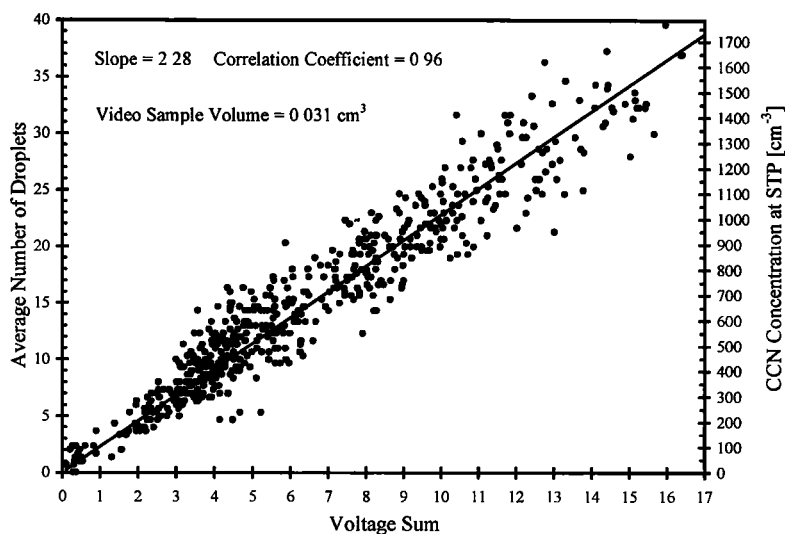


Figure 2. Plot of the photodetector voltage sum versus the number of cloud condensation nuclei within the video sample volume. Data from six independent calibration runs, of 100 air samples each, are shown. NaCl aerosol is used during calibration.

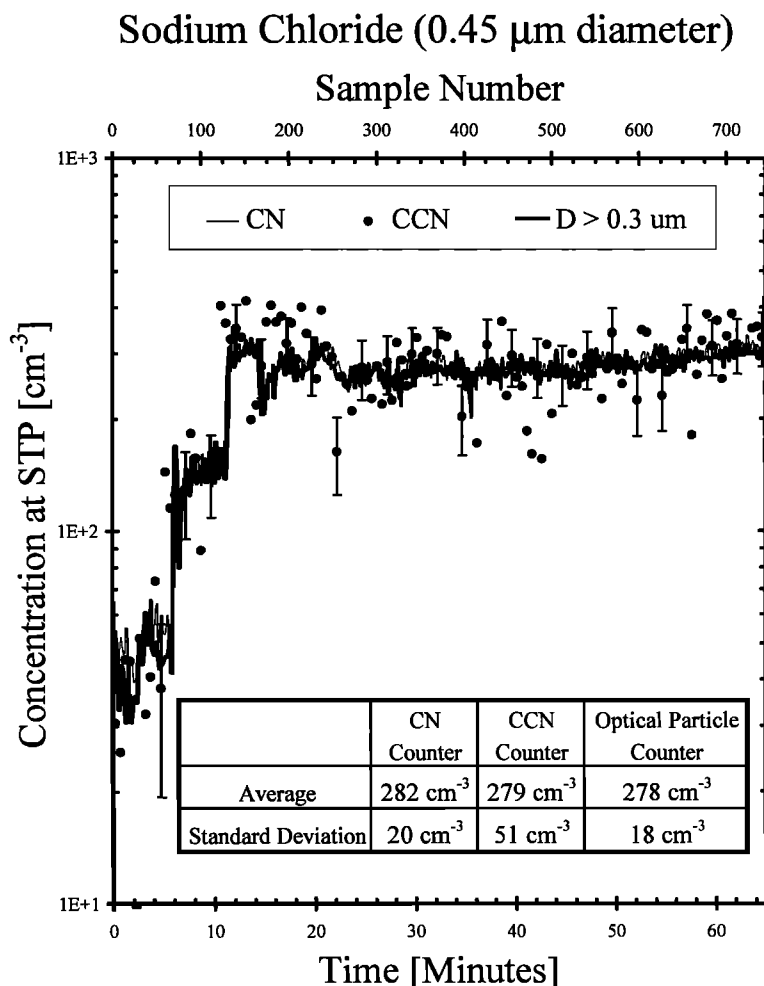


Figure 3. Comparison of measurements of a monodisperse NaCl aerosol by an optical particle counter, the CCN counter, and a CN counter. The table gives the mean concentrations and standard deviation between 20 and 65 min for the laboratory data shown. Concentrations are given at standard temperature and pressure.

droplet. A group of pixels above the threshold and totally surrounded by pixels below the threshold is defined as one drop. This approach is limited to concentrations that have a negligible number of droplet coincidences. The brightness threshold value is set at the start of a calibration run, when no activated CCN are present, as the brightest value still yielding zero particles within the video sample volume. Therefore the brightness threshold value takes into account the inherent noise of the video system, which was found to remain constant if the temperature of the video camera did not change.

Figure 1 shows an original video frame and a processed frame (after thresholding). The computer algorithm counted 35 droplets in this image, in agreement with manual counting. Some additional bright pixels seen in the gray scale image fell below the detection level and were therefore considered noise. Many of the droplets seen in Figure 1 consist of only a few pixels, and some droplets consist of only one pixel. A video camera with improved resolution might further improve the accuracy of the calibration procedure.

Since the photodetector baseline may drift between samples, the photodetector voltage is corrected by subtracting the average photodetector voltage during the chamber flush.

This subtraction also takes out effects of light scattering by air molecules which change with pressure and temperature. Several methods, besides the traditional approach of using data at the moment of maximum droplet concentration, were considered for evaluating the time-varying photodetector output and droplet counts. This is necessary since the scattered light intensity is determined not only by droplet numbers but also by the sizes of the droplets and their locations with respect to an imperfectly uniform illumination. Furthermore, both the detector output and the video counts are subject to random sampling errors. A droplet's size and fall speed may be influenced by the initial size of the CCN; however, the narrowing of the droplet spectrum during growth will act to minimize variation in droplet size. Future laboratory work is planned to investigate the dependence of the photodetector calibration on CCN size.

In a search for the most robust calibration method possible, we evaluated numerous methods of characterizing the photodetector signal pulse and relative timing of the video count. Results were found to be relatively insensitive to the method of evaluation ($\sim 5\%$). The following calibration method was chosen based on the highest correlation coefficient. The peak voltage is found, and the voltages from

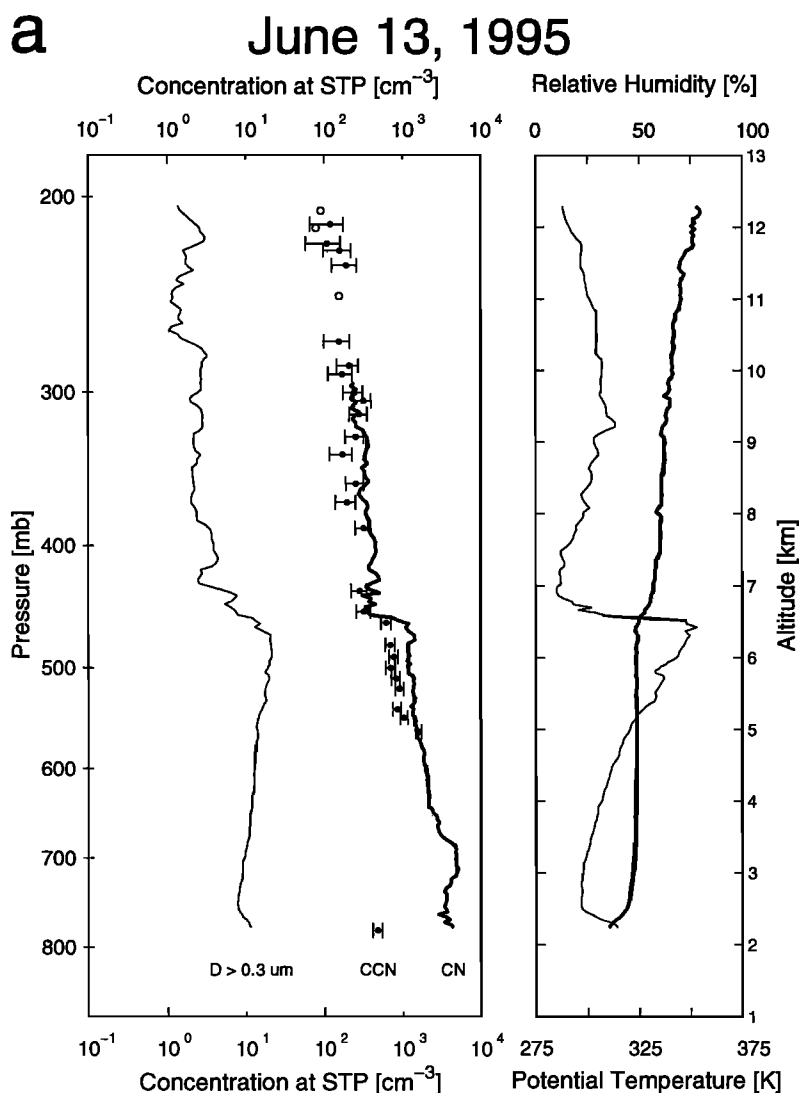


Figure 4. Four representative ascent profiles for early morning balloon flights at Laramie, Wyoming. Each profile includes the smallest size channel of the optical particle counter ($D > 0.3 \mu\text{m}$, thin line), the CCN concentration (circles), and the CN concentration ($D > 0.01 \mu\text{m}$, thick line). Open circles represent measurements below the detection limit of the CCN counter. The concentration measured by each instrument has been corrected to standard temperature and pressure. Potential temperature (thick line) and relative humidity (thin line) are shown in the right-hand panel.

the preceding and following seconds are added to it. The number of droplets is defined as the average of the droplets counted over the same time interval. The calibration data and a least squares linear fit are shown in Figure 2. The slope of the regression line and video sample volume are used to determine the CCN concentration. Since zero droplets in the chamber should produce no scattered light, the straight line fit was forced to have a zero y intercept. The aerosol used in the calibration was produced from a solution of NaCl (1.0 g/L) by an ultrasonic vaporizer. The concentration of CCN was varied by changing the amount of clean air mixed with the generated aerosol.

One of the most important factors during the calibration procedure is the focus setting of the lens. Small adjustments of the focus setting could have up to a 30% effect on the calibration constant. The reason for this sensitivity is that out

of focus bright particles will run together reducing particle count, and out of focus dim particles are not bright enough to be counted. An optimum focus setting was determined based on the highest droplet count at a given photodetector voltage. When the optimum focus for the chosen video sample volume was obtained, it was fixed for all data runs.

The advantages of the video camera calibration procedure are that it may be done fairly quickly and requires only a moderate amount of additional equipment; however, it is subject to possible systematic errors in lens adjustment and in the determination of video sample volume. Following *Gras* [1995], we checked our calibration results by making simultaneous measurements of a monodisperse NaCl aerosol with our CCN counter, a condensation nucleus (CN) counter [*Rosen and Hofmann*, 1977] and an optical particle counter sensitive to particles greater than $0.3 \mu\text{m}$ diameter ($D_{0.3}$)

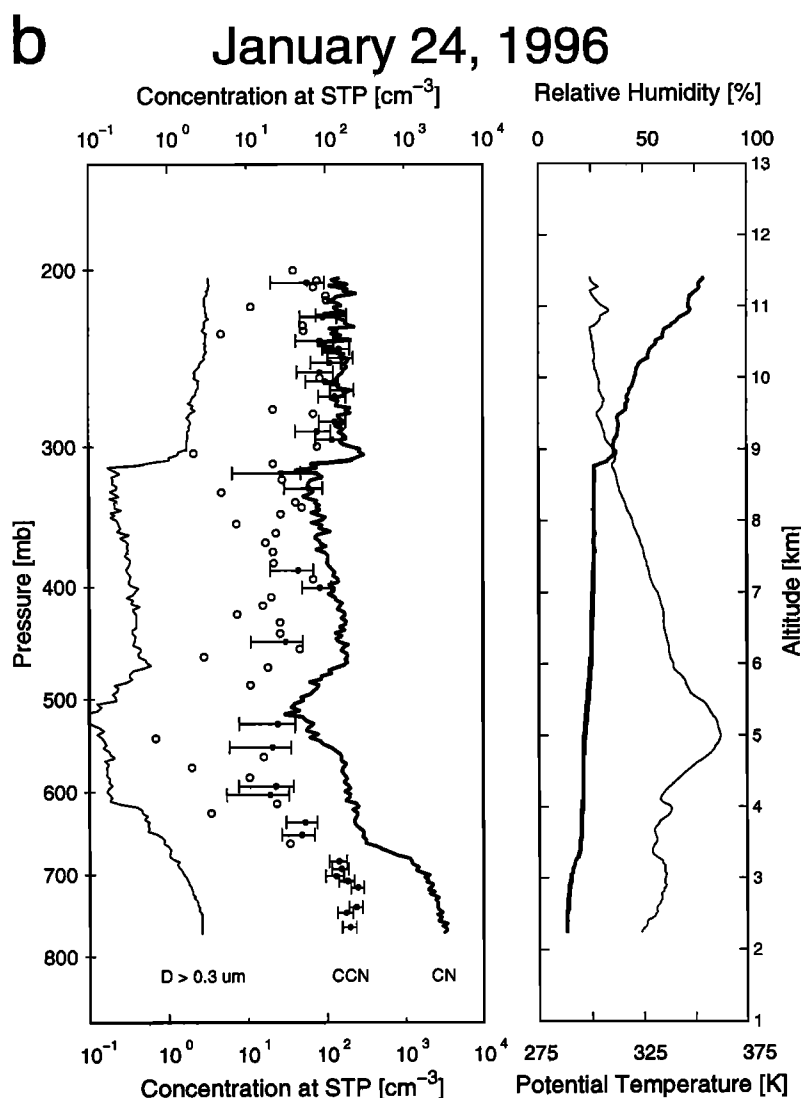


Figure 4. (continued)

[Hofmann, *et al.*, 1975]. The monodisperse NaCl aerosol was produced using an electrostatic classifier [Knutson and Whitby, 1975]. Figure 3 shows the results obtained with aerosols of $0.45 \mu\text{m}$ mean diameter. NaCl particles of $0.45 \mu\text{m}$ diameter are more than 10 times larger than the critical activation size at 1% supersaturation and was chosen so that the comparison could include the optical particle counter. Agreement among the three counters is excellent and indicates that all the NaCl particles have activated at 1% supersaturation as expected.

The table in Figure 3 gives the average and standard deviation of the number concentrations between 20 and 65 min. Average values show agreement within 1% for the optical particle counter, the CCN counter, and the CN counter. The CCN concentration is more variable than the CN concentration or the optical particle concentration. This is not surprising, since both the CN counter and the optical particle counter are continuous flow instruments where each data point represents an average over 10 s and thousands of particles. The CCN counter produces one measurement every

30 s and counts fewer particles (at the same concentration) than the CN counter or the optical particle counter.

An estimate for the relative error in CCN concentration is computed based on the Poisson counting error for the number of particles detected by the photodetector. The Poisson counting error is given by the square root of the number of particles counted. The length of the laser beam over which the photodetector is sensitive to scattered light was estimated to be 5 cm by moving a scattering target through the beam. This length and the $4 \times 1 \text{ mm}$ elliptical crosssection of the beam yield a photodetector sample volume of 0.16 cm^3 . Thus for a CCN concentration of 278 cm^{-3} the Poisson counting error is 50 cm^{-3} or 18%. The observed standard deviation of CCN concentrations (see table in Figure 3) is well accounted for by random sampling errors.

The detection limit of the CCN counter is defined by requiring that the three photodetector voltages used for the voltage sum exceed by two standard deviations the average voltage during chamber flush, and the time of the photodetector voltage peak has to occur within two standard

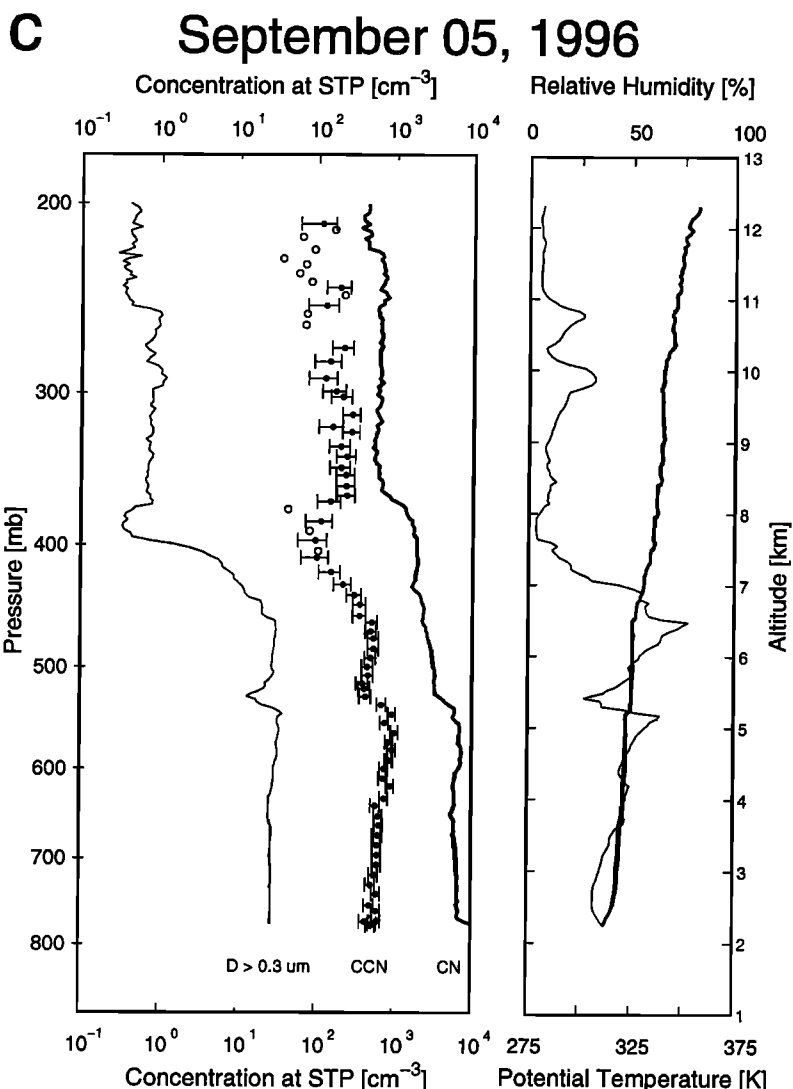


Figure 4. (continued)

deviations, 3 s, of the time when the mean photodetector voltage peak occurred during calibration. This removes noise peaks that occur at times inconsistent with the activation and growth of CCN at 1% supersaturation. Using these two criteria, filtered air produced no accepted measurements. The detection limit criteria are conservative, so some valid measurements may be rejected.

4. Midlatitude Continental Aerosol Profiles

Balloon flights at Laramie, Wyoming, start at dawn with clear skies and last for 2 to 3 hours. During the flight the CCN counter is operated at a constant supersaturation of 1%. Although the balloon package ascends to a pressure of about 10 mbar, the CCN counter is switched off at a pressure of 200 mbar to avoid overheating due to reduced heat transfer at low pressures. In addition to the CCN counter, the instrument package also contains an optical particle counter, a CN counter (aerosols $D > 10 \text{ nm}$), a nephelometer, and a radiosonde unit (VAISALA) to measure pressure, temperature, and humidity. The aerosol instruments share a

common inlet that is fitted with a heater. The heater maintains the inlet air temperature at 40°C during ascent and at 160°C during descent. In this paper, only the ascent data will be discussed. After the heated inlet, the air flows through 0.6–1 m of stainless steel tubing to each instrument. Although the air cools between the heated inlet and the instruments, it remains well above the ambient temperature, so the relative humidity of the air entering each instrument remains low. Therefore each instrument measures dry aerosol particles.

Figure 4 shows four representative examples of data from our current set of nine ascent profiles. Included in each profile are concentrations of CN, CCN, aerosol with $D > 0.3 \mu\text{m}$, ambient potential temperature, and relative humidity. Aerosol concentrations have been corrected to standard temperature and pressure (STP). The missing CCN data below 550 mbar in the June 13, 1995, profile was due to instrument problems (differential temperature not within the temperature tolerance). CCN concentrations that did not exceed the detection limit (defined earlier) are given by open circles. Error bars for CCN concentrations are computed based on Poisson counting error for the number of droplets

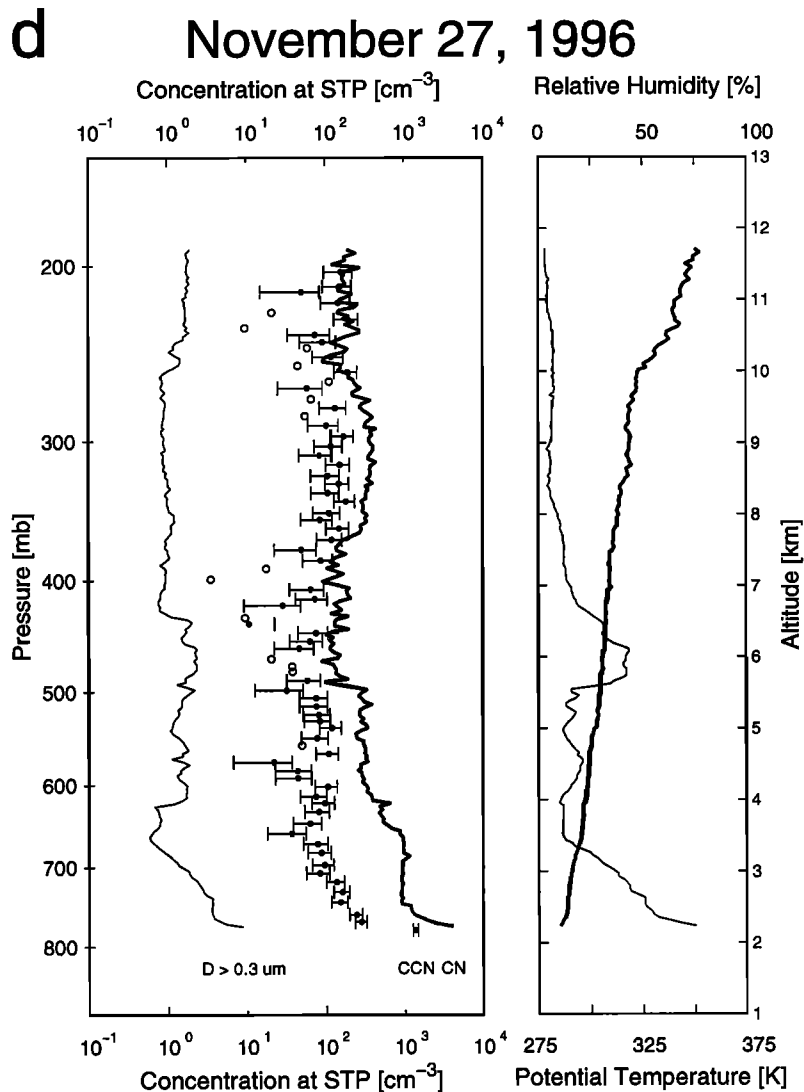


Figure 4. (continued)

detected by the photodetector. The absolute accuracy of the balloon aerosol counters using the heated inlet under flight conditions has not been fully determined so far. Thus the concentrations shown in Figure 4 should be considered preliminary results. Some patterns observed in the available profiles deserve comment and are summarized below. Most of these observations are evident in the examples included in Figure 4. Please note that these observations are based on only nine balloon flights from a single location.

1. The decrease of CCN concentration in the upper troposphere as compared to the lower troposphere agrees with previous studies [Hoppel *et al.*, 1973; Raga and Jonas, 1995] and indicates a source within the lower troposphere or at the Earth's surface for continental air masses.

2. CCN concentrations are lower in winter than in summer. The January 24, 1996, profile, Figure 4b, shows CCN concentration $< 200 \text{ cm}^{-3}$, whereas the summer profiles, Figures 4a and 4c, show concentrations $> 200 \text{ cm}^{-3}$ up to about 500 mbar. This observation is consistent with the surface observations of Hudson and Frisbie [1991] near Reno, Nevada.

3. The CN measurements near the surface agree with the surface observation of Hudson and Frisbie [1991] in showing little seasonal changes. However, the CN profiles decrease much more rapidly in winter than summer. This seasonal trend in CN concentration has been previously noted by Hofmann [1993].

4. The CCN to CN concentration ratio is sometimes nearly 1 (Figure 4a), and at other times it is as small as 0.1 (Figure 4c). This range of ratios appears to hold for all altitudes.

5. The CCN to CN concentration ratio typically increased with height.

6. An increase in aerosol concentration and an increase in the CCN to CN concentration ratio above the tropopause were observed (see Figure 4b at 8.5 km). Measured ozone concentration was used to define the tropopause.

7. At times there was a factor of 10 decrease in CCN concentration in the first 0.5 km above the surface (Figure 4d); however, often the CCN concentration remained constant for several kilometers (Figure 4c) above the surface. Convectively driven mixing on the preceding days is the likely explanation for this. Such profiles support the

assumption that surface CCN concentrations are representative of the concentrations at cloud base, as noted by Hudson [1982].

8. Variations in CCN concentration over the height interval of 0.5 to 2 km were usually accompanied by parallel variations in CN, $D_{0.3}$ and relative humidity (see Figure 4a at 6.5 km and Figure 4c at 5.5 km). The majority of such local changes were decreases in all parameters and frequently occurred within layers of increased stability. An example of the opposite pattern, an increase in CN while other parameters decrease, is observed at 7.5 km in Figure 4c.

5. Conclusions

A new light-weight static thermal gradient CCN counter has been developed for balloon-borne measurements utilizing a photodetector to measure droplet concentrations. A calibration method has also been developed based on simultaneous determination of droplet concentrations using the photometric detector and a video system. Comparison was made between the CCN counter and two independent particle counters using monodisperse NaCl test aerosol. To date, nine balloon flights carrying the new CCN counter have been successfully completed from Laramie, Wyoming, a midcontinental location. These flights provided a first data set on vertical profiles of CCN through the entire depth of the troposphere.

Acknowledgments. Lyle Womack and Jason Gonzales provided technical support in conducting balloon flight measurements and laboratory work. We appreciate the work of two reviewers who greatly improved this manuscript with their helpful suggestions. This research was supported by a grant from the National Aeronautics and Space Administration.

References

- Bartlett, B. M., and G. P. Ayers, Static diffusion cloud chamber, *J. Rech. Atmos.*, **15**, 231-233, 1981.
- Elliott, W. P., Dimensions of thermal diffusion chambers, *J. Atmos. Sci.*, **28**, 810-811, 1971.
- Gras, J. L., CN, CCN and particle size in Southern Ocean air at Cape Grim, *Atmos. Res.*, **35**, 233-251, 1995.
- Hegg, D. A., R. J. Rerek, and P. V. Hobbs, Cloud condensation nuclei over the Arctic Ocean in early spring, *J. Appl. Meteorol.*, **34**, 2076-2082, 1995.
- Hobbs, P. V., *Aerosol-Cloud-Climate Interactions*, pp. 33-73, Academic, San Diego, Calif., 1993.
- Hofmann, D. J., Twenty years of balloon-borne tropospheric aerosol measurements at Laramie, Wyoming, *J. Geophys. Res.*, **98**, 12,753-12,766, 1993.
- Hofmann, D. J., J. M. Rosen, T. J. Pepin, and R. G. Pinnick, Stratospheric aerosol measurements I, Time variations at northern midlatitudes, *J. Atmos. Sci.*, **32**, 1446-1436, 1975.
- Hoppel, W. A., and T. A. Wojciechowski, Description and discussion of the NRL TGDCC, *J. Rech. Atmos.*, **15**, 209-213, 1981.
- Hoppel, W. A., J. E. Dinger, and R. R. Ruskin, Vertical profiles of CCN at various geographical locations, *J. Atmos. Sci.*, **30**, 1410-1420, 1973.
- Hudson, J. G., Correlation between surface and cloud base CCN spectra in Montana, *J. Appl. Meteorol.*, **21**, 1427-1440, 1982.
- Hudson, J. G., Cloud condensation nuclei, *J. Appl. Meteorol.*, **32**, 596-607, 1993.
- Hudson, J. G., and P. Squires, Continental surface measurements of CCN flux, *J. Atmos. Sci.*, **35**, 1289-1295, 1978.
- Hudson, J. G., and P. R. Frisbie, Surface cloud condensation nuclei and condensation nuclei measurements at Reno, Nevada, *Atmos. Environ.*, **25(A)**, 2285-2299, 1991.
- Hudson, J. G., and G. Svensson, Cloud microphysical relationships in California marine stratus, *J. Appl. Meteorol.*, **34**, 2655-2666, 1995.
- Katz, J. L., and P. Mirabel, Calculation of supersaturation profiles in thermal diffusion cloud chambers, *J. Atmos. Sci.*, **32**, 646-652, 1975.
- Knutson, E. O. and K. T. Whitby, Aerosol classification by electric mobility: Apparatus, theory, and applications, *J. Aerosol Sci.*, **6**, 443-451, 1975.
- Jennings, S. G., *Aerosol Effects on Climate*, pp. 275-297, Univ. of Arizona Press, Tucson, 1993.
- Lala, G. G., An automatic light scattering CCN counter, *J. Rech. Atmos.*, **15**, 259-262, 1981.
- Lala, G. G., and J. E. Jiusto, An automatic light scattering CCN counter, *J. Appl. Meteorol.*, **16**, 413-418, 1977.
- Raga, G. B., and P. R. Jonas, Vertical distribution of aerosol particles and CCN in clear air around the British Isles, *Atmos. Environ.*, **29**, 673-684, 1995.
- Rosen, J. M. and D. J. Hofmann, Balloonborne measurements of condensation nuclei, *J. Appl. Meteorol.*, **16**, 56-62, 1977.
- Twomey, S., Aerosols, clouds and radiation, *Atmos. Environ.*, **25(A)**, 2435-2442, 1991.
- Wigley, T. M. L., Possible climate change due to SO_2 -derived cloud condensation nuclei, *Nature*, **339**, 365-367, 1989.
- D. J. Delene, T. Deshler, P. Wechsler, and G. A. Vali, Department of Atmospheric Sciences, University of Wyoming, P.O. Box 3038, Laramie, WY 82071-3038. (e-mail: delene@grizzly.uwyo.edu; deshler@grizzly.uwyo.edu; wex@grizzly.uwyo.edu; vali@grizzly.uwyo.edu)

(Received June 3, 1997; revised December 22, 1997; accepted December 23, 1997.)